Available online at www.sciencedirect.com
ScienceDirect
Journal of Solid State Chemistry 181 (2008) 828–836
JOURNAL OF SOLID STATE CHEMISTRY
www.elsevier.com/locate/jssc

Topologically novel copper molybdate phases based on 3,4′-dipyridylketone: Hydrothermal synthesis, structural characterization, and magnetic properties

Matthew R. Montney, Robert L. LaDuca*

Lyman Briggs College and Department of Chemistry, E-30 Holmes Hall, Michigan State University, East Lansing, MI 48825, USA

Received 8 October 2007; received in revised form 17 January 2008; accepted 21 January 2008
Available online 6 February 2008

Abstract

Hydrothermal treatment of $CuCl_2 \cdot 2H_2O$, MoO_3, and 3,4′-dipyridylketone (3,4′-dpk) in 1:1:2 mole ratio afforded the new mixed metal oxide phases $[Cu_2(MoO_4)_2(3,4'\text{-dpk})(H_2O)]$ (**1**) or $[Cu_4(3,4'\text{-dpk})_4(Mo_8O_{26})]$ (**2**), depending on the pH of the initial reaction mixture. Compound **1** possesses unique one-dimensional (1-D) $[Cu_2(MoO_4)_2(H_2O)]_n$ ribbons constructed from the linkage of $\{Cu^{II}_4O_6\}$ tetrameric units through isolated $[MoO_4]^{2-}$ tetrahedra. These ribbons in turn are connected into a two-dimensional (2–D) coordination polymer structure by tethering 3,4′-dpk ligands. Compound **2**, containing monovalent copper ions, manifests an unprecedented "X-rail" 1-D extended structure with $(6^28)_4(6^6)$ topology formed from the bracketing of discrete $[\beta\text{–}Mo_8O_{26}]^{4-}$ anions by four $[Cu^I(3,4'\text{-dpk})]^{n+}_n$ chains. The variable temperature magnetic susceptibility behavior of **1** was fit to a linear tetramer model, with $g = 2.03(3)$, $J_1 = 25.8(7)\,cm^{-1}$ and $J_2 = -46(1)\,cm^{-1}$. Antiferromagnetic inter-tetramer interactions ($zJ' = -0.21(3)\,cm^{-1}$) were also evident. Crystallographic data: **1** monoclinic, $P2_1/c$, $a = 10.3911(11)$ Å, $b = 6.9502(6)$ Å, $c = 22.958(2)$ Å, $\beta = 100.658(7)^\circ$, $V = 1629.5(3)$ Å^3, $R_1 = 0.1256$, and $wR_2 = 0.2038$; **2** triclinic, $P\bar{1}$, $a = 10.9000(3)$ Å, $b = 11.7912(4)$ Å, $c = 13.5584(4)$ Å, $\alpha = 102.482(2)^\circ$, $\beta = 102.482(2)^\circ$, $\gamma = 117.481(2)^\circ$, $V = 1450.98(8)$ Å^3, $R_1 = 0.0428$, and $wR_2 = 0.0630$.

keywords: Copper; Polyoxomolybdate; Coordination polymer; Magnetism; Crystal structure; Dipyridylketone

1. Introduction

Solid-state metal oxides have commercial utility in a variety of applications, from structural engineering materials to more technologically advanced products in the microelectronics industry such as laser waveguides and piezoelectrics [1]. The underlying atomic-level structure plays an extremely significant role in the resulting macroscopic properties of these materials. Much research has been undertaken towards the rational design and fabrication of solid-state oxide nanostructures with deliberately tailored properties [2]. Nevertheless, exploratory synthetic efforts continue to advance the structural complexity and potential applications of solid-state oxide materials. One recent approach towards the synthesis of new mixed metal oxide phases has been the hydrothermal self-assembly of copper molybdate substructures in the presence of tethering or chelating organodiimines [3–11].

Within these hybrid materials, the secondary transition metal ions provide the necessary charge balance and points of contact for the connection of polyoxomolybdate anionic clusters or chains into extended frameworks. The donor disposition and steric constraints imposed by the organodiimine ligand can exert significant structure directing effects during the self-assembly of copper polyoxomolybdate hybrid solids. Thus, a wide diversity of structural motifs can be generated through variance of the organodiimine even in cases where the largest polyoxometallates are only $[MoO_4]^{2-}$ tetrahedra. For instance, $\{[Cu(4,4'\text{-bpy})_{0.5}MoO_4] \cdot 1.5H_2O\}$ manifests two-dimensional (2-D) $[CuMoO_4]$ layers containing $\{MoO_4\}$

*Corresponding author.
E-mail address: laduca@msu.edu (R.L. LaDuca).

0022-4596/$ - see front matter © 2008 Elsevier Inc. All rights reserved.
doi:10.1016/j.jssc.2008.01.036

tetrahedra and $\{Cu_4O_6\}$ tetramers formed from edge-sharing $\{CuO_5N\}$ octahedra, all linked into three-dimensions (3-D) through rigid-rod tethering 4,4′-bpy ligands. However, in [Cu(3,4′-bpy)MoO_4] (3,4′-bpy = 3,4′-bipyridine), $\{MoO_4\}$ tetrahedra and $\{CuN_2O_3\}$ square pyramids engage in corner-sharing to construct layers composed of $\{Cu_3Mo_3O_6\}$ ring-shaped subunits. In turn, these are strutted by the kinked donor disposition ligand 3,4′-bpy to form a unique 3-D polymeric network [3].

In copper/molybdate/organodiimine hybrid materials featuring larger polyoxometallate anions, no fewer than seven different octamolybdate isomeric variants have been isolated, again through the employment of organic components with different donor dispositions and conformational flexibility. For example, the 2-D layered phases [{Cu(bpe)}$_4Mo_8O_{26}$] (bpe = 1,2-bis-(4-pyridyl)ethylene) [4] and [Cu_4(dpp)$_4Mo_8O_{26}$] (dpp = 1,3-di-4-pyridylpropane) [5] exhibited the α-octamolybdate isomer, while the 2-D coordination polymers [{Cu(pyridine)}$_4Mo_8O_{26}$] [6] and [Cu_2(2,4′-bpy)$_2Mo_8O_{26}$] [7] adopt the more densely arranged [β-Mo_8O_{26}]$^{4-}$ isomer. Use of the rigid-rod donor 4,4′-bipyridine (4,4′-bpy) resulted in the 2-D coordination polymer [Cu_4(4,4′-bpy)$_4Mo_8O_{26}$] [8], which manifested the rarely seen δ octamolybdate isomer. The exotetradentate ligand tetra-4-pyridylpyrazine (tpyrpyz) was recently used to generate the 3-D phase [{Cu_2(tpyrpyz)}$_2Mo_8O_{26}$] [9] featuring the ζ octamolybdate isomer, which is based on equal numbers of coordination octahedra and square pyramids.

Herein we describe the hydrothermal synthesis and structural determinations of two hybrid copper molybdate phases incorporating the kinked exobidentate organodiimine 3,4′-dipyridylketone (3,4′-dpk), [$Cu_2(MoO_4)_2$(3,4′-dpk)(H_2O)] (**1**) and [Cu_4(3,4′-dpk)$_4$(Mo_8O_{26})] (**2**). While **1** manifests a unique 2-D layered structure containing one-dimensional (1-D) [$Cu_2(MoO_4)_2$] ribbons built from tetranuclear $\{Cu^{II}_4O_6\}$ clusters, the Cu^I-containing phase **2** possesses an unprecedented 1-D "X-rail" morphology built from the bracketing of [β-Mo_8O_{26}]$^{4-}$ anions by $[Cu(3,4'\text{-dpk})]^{2n+}_n$ chains. The variable temperature magnetic behavior of **1** was also measured and modeled successfully using a linear tetramer model. To the best of our knowledge **1** and **2** represent the first metal-organic materials to incorporate 3,4′-dpk.

2. Experimental section

2.1. General considerations

Copper(II) chloride dihydrate and molybdenum(VI) oxide were obtained from Fisher and Acros, respectively. 3,4′-dpk was prepared via the reaction of 3-lithiopyridine with methyl isonicotinate in a similar manner to that reported by Mak for the preparation of 3,3′-dpk [12]. Water was deionized above 3 MΩ in-house. IR spectra were recorded on a Perkin Elmer Spectrum One instrument on ground powdered samples. Variable temperature magnetic susceptibility data (2–300 K) was collected on a Quantum Design MPMS SQUID magnetometer at an applied field of 0.1 T. After each temperature change the sample was kept at the new temperature for 5 min before magnetization measurement to ensure thermal equilibrium. The susceptibility data was corrected for diamagnetism using Pascal's constants [13].

2.2. Preparation of [$Cu_2(MoO_4)_2$(3,4′-dpk)(H_2O)] (**1**)

$CuCl_2 \cdot 2H_2O$ (63 mg, 0.37 mmol), MoO_3 (53 mg, 0.37 mmol), and 3,4′-dpk (136 mg, 0.74 mmol) were placed into 10 g (555 mmol) distilled H_2O in a Teflon-lined 23 mL Parr acid digestion bomb. The bomb was sealed and heated at 120 °C for 44 h, whereupon it was cooled slowly in air to 25 °C. Green crystals of **1** (76 mg, 63% yield based on Cu) were isolated after washing with distilled water and acetone and drying in air. Anal. for $C_{11}H_{10}Cu_2Mo_2N_2O_{10}$ (**1**): Calc. C 20.35, H 1.55, N 4.32%, Found C 20.65, H 1.46, N 4.65%. IR (cm^{-1}): 3588 w, 3319 w br, 3086 w, 3054 w, 3017 w, 1667 m, 1638 m, 1607 m ,1571 w, 1545 w, 1420 m, 1347 w, 1333 m, 1298 m, 1228 w, 1204 m, 1167 w, 1131 w, 1067 w, 1032 w, 953 w, 939 w, 914 m, 895 m, 877 m, 861 m, 825 m, 779 s, 731 s, 657 s.

2.3. Preparation of [Cu_4(3,4′-dpk)$_4$(Mo_8O_{26})] (**2**)

The preparative procedure for **1** was followed with the exception of the addition of 0.5 mL 1.0 M NaOH solution prior to heating. Dark red crystals of **2** (79 mg, 39% yield based on Cu) were isolated after washing with distilled water and acetone and drying in air. Anal. for $C_{44}H_{32}Cu_4Mo_8N_8O_{30}$ (**2**): Calc. C 24.30, H 1.48, N 5.15%, Found C 25.51, H 1.48, N 5.53%. IR (cm^{-1}): 3017 w, 1676 m, 1658 m, 1594 m, 1546 m, 1471 w, 1413 m, 1320 m, 1281 m, 1164 w, 1060 w, 1028 w, 942 m, 898 m, 877 s, 831 m, 818 m, 750 m, 703 s, 690 s, 655 s.

3. X-ray crystallography

Single crystals of **1** and **2** were subjected to single-crystal X-ray diffraction at 173 K using a Bruker-AXS Apex II CCD instrument. Reflection data was acquired using graphite-monochromated Mo-$K\alpha$ radiation ($\lambda = 0.71073$ Å). The data was integrated via SAINT [14]. Lorentz and polarization effect and absorption corrections were applied with SADABS [15]. The structures were solved using direct methods and refined on F^2 using SHELXTL [16]. All non-hydrogen atoms were refined anisotropically. Hydrogen atoms bound to carbon atoms were placed in calculated positions and refined isotropically with a riding model. Hydrogen atoms belonging to the bound water molecule in **1** were located via Fourier difference map, restrained at fixed positions, and refined isotropically. Supramolecular contacts (hydrogen bonding, $\pi-\pi$ stacking) were probed and calculated using PLATON [17]. Relevant crystallographic data for **1** and **2** are listed in Table 1.

4. Results and discussion

4.1. Synthesis and spectral characterization

Compound **1** was prepared cleanly under hydrothermal conditions by reaction of copper chloride, molybdenum (VI) oxide and 3,4′-dpk in a 1:1:2 mole ratio, with no adjustment of pH. Elevated pH levels promoted reduction to monovalent copper in this system, affording compound **2** under similar hydrothermal conditions. The infrared spectra of **1** and **2** were consistent with their single-crystal X-ray structures. Sharp, medium intensity bands in the range from ~1600 to ~1200 cm^{-1} were ascribed to stretching modes of the pyridyl rings of the 3,4′-dpk moieties. Bands in the region of 1635–1680 cm^{-1} marked the presence of the C = O stretching frequencies of the ketone functional groups of the 3,4′-dpk ligands. Features corresponding to pyridyl ring puckering mechanisms were evident in the region between 800 and 670 cm^{-1}. Bands consistent with vibrational modes of Mo = O, Mo–O–Mo, and Cu–O–Mo units occurred in the spectral region between 960 and 800 cm^{-1}.

Table 1
Crystal and structure refinement data

Data	**1**	**2**
Empirical formula	$C_{11}H_{10}Cu_2Mo_2N_2O_{10}$	$C_{44}H_{32}Cu_4Mo_8N_8O_{30}$
Formula weight	649.17	2174.48
Crystal morphology	Green plate	Red block
Crystal size (mm)	0.22 × 0.12 × 0.04	0.28 × 0.24 × 0.14
Collection T (K)	173(2)	173(2)
λ (Å)	0.71073	0.71073
Crystal system	Monoclinic	Triclinic
Space group	$P2_1/c$	$P\bar{1}$
a (Å)	10.3911(11)	10.9000(3)
b (Å)	6.9502(6)	11.7912(4)
c (Å)	22.958(2)	13.5584(4)
α (°)	90	97.987(2)
β (°)	100.658(7)	102.482(2)
γ (°)	90	117.481(2)
V (Å^3)	1629.5(3)	1450.98(8)
Z	4	1
D_{calc} (g cm^{-3})	2.646	2.489
μ (mm^{-1})	4.138	3.196
Min/max trans.	0.477	0.859
$h\,k\,l$ ranges	$-9 \leqslant h \leqslant 9$	$-11 \leqslant h \leqslant 11$,
	$-10 \leqslant k \leqslant 10$	$-13 \leqslant k \leqslant 13$
	$-21 \leqslant l \leqslant 21$	$-18 \leqslant l \leqslant 18$
Total reflections	12,857	46,820
Unique reflections	3573	11381
R(int)	0.0907	0.0371
Parameters/restraints	227/3	425/0
R_1 (all data)	0.1253	0.0428
R_1 ($I > 2\sigma(I)$)	0.0739	0.0273
wR_2 (all data)	0.2034	0.0630
wR_2 ($I > 2\sigma(I)$)	0.1738	0.0559
Max/min residual (e$^-$/Å^3)	2.502/–2.286	0.820/–0.873
G.O.F.	1.082	1.004

4.2. Structural description of $[Cu_2(MoO_4)_2(3,4'\text{-dpk})(H_2O)]$ (1)

Compound **1** crystallized in the monoclinic space group $P2_1/c$ with an asymmetric unit containing two divalent copper atoms, two dianionic molybdate units, one water molecule bound to Cu1, and one complete 3,4′-dpk molecule (Fig. 1). The coordination environments around both crystallographically distinct molybdenum atoms are slightly distorted {MoO_4} tetrahedra. However, while Mo1 bears only one terminal Mo = O unit, Mo2 has two. One copper atom (Cu1) possesses a distorted square pyramidal ($\tau = 0.20$) [18] {CuO_4N} coordination geometry, with three oxygen donors belonging to three different molybdate anions and one nitrogen donor (N1) from a 3,4′-dpk ligand situated in the basal plane. The apical position is occupied by an aquo ligand (O10) with a longer bond length to Cu1. The bond lengths and angles at Cu1 are consistent with the Jahn–Teller active d^9 electronic configuration of divalent copper. On the other hand, the second crystallographically

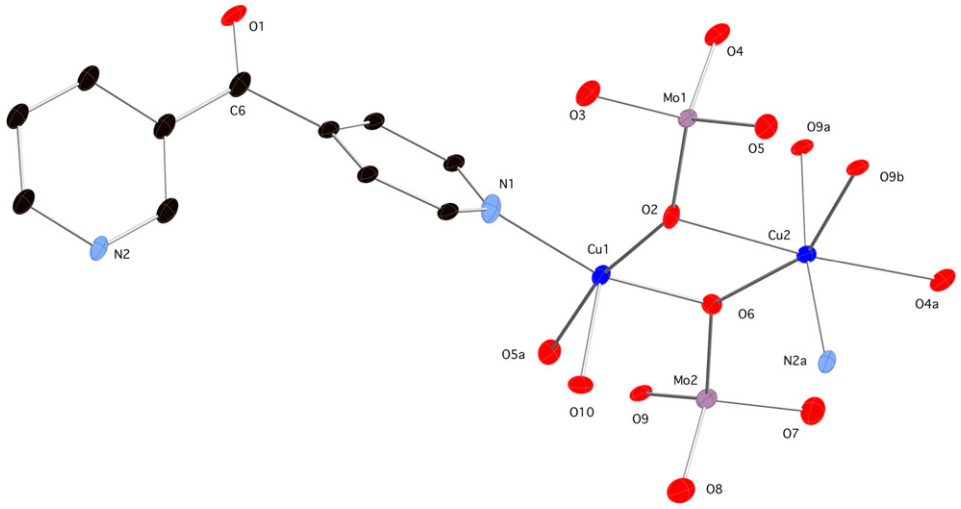

Fig. 1. Coordination environments in **1**, with thermal ellipsoids shown at 50% probability and partial atom numbering scheme. Hydrogen atoms have been omitted.

Table 2
Selected bond distance (Å) and angle (°) data for **1**

Cu1–O2	1.956(7)	O2–Cu1–O6	87.4(3)
Cu1–O6	1.972(8)	O2–Cu1–O5$^{\#1}$	168.6(3)
Cu1–O5$^{\#1}$	1.978(7)	O6–Cu1–O5$^{\#1}$	83.4(3)
Cu1–N1	2.004(10)	O2–Cu1–N1	95.9(3)
Cu1–O10	2.271(8)	O6–Cu1–N1	156.7(4)
Cu2–O6	1.945(7)	O5$^{\#1}$–Cu1–N1	95.2(3)
Cu2–O9$^{\#2}$	1.980(7)	O2–Cu1–O10	87.4(3)
Cu2–N2$^{\#3}$	1.996(10)	O6–Cu1–O10	105.1(3)
Cu2–O9$^{\#4}$	2.003(8)	O5$^{\#1}$–Cu1–O10	88.4(3)
Cu2–O4$^{\#5}$	2.352(8)	N1–Cu1–O10	98.1(4)
Cu2–O2	2.467(8)	O6–Cu2–O9$^{\#2}$	153.8(3)
Mo1–O3	1.712(8)	O6–Cu2–N2$^{\#3}$	95.2(3)
Mo1–O4	1.716(9)	O9$^{\#2}$–Cu2–N2$^{\#3}$	98.4(3)
Mo1–O2	1.792(7)	O6–Cu2–O9$^{\#4}$	89.2(3)
Mo1–O5	1.811(7)	O9$^{\#2}$–Cu2–O9$^{\#4}$	80.0(3)
Mo2–O8	1.698(9)	N2$^{\#3}$–Cu2–O9$^{\#4}$	172.6(4)
Mo2–O7	1.713(9)	O6–Cu2–O4$^{\#5}$	110.8(3)
Mo2–O9	1.854(8)	O9$^{\#2}$–Cu2–O4$^{\#5}$	92.1(3)
Mo2–O6	1.872(7)	N2$^{\#3}$–Cu2–O4$^{\#5}$	87.7(3)
		O9$^{\#4}$–Cu2–O4$^{\#5}$	85.2(3)
		O6–Cu2–O2	74.9(3)
		O9$^{\#2}$–Cu2–O2	82.0(3)
		N2$^{\#3}$–Cu2–O2	93.2(3)
		O9$^{\#4}$–Cu2–O2	93.7(3)
		O4$^{\#5}$–Cu2–O2	174.1(3)
		Cu1–O2–Cu2	90.3(3)
		Cu2–O6–Cu1	107.4(4)

Symmetry equivalent atoms: (#1) x, $y+1$, z; (#2) x, $y-1$, z; (#3) $-x+1$, $y-1/2$, $-z+1/2$; (#4) $-x+1$, $-y+1$, $-z+1$; (#5) $-x+1$, $-y$, $-z+1$.

distinct copper atom (Cu2) possesses a distorted octahedral $\{CuO_5N\}$ coordination environment, with one oxygen atom from each of five different molybdate dianions and one nitrogen atom (N2) from a 3,4′-dpk comprising the roster of donor atoms. The long *trans* bonds (Cu2–O2, Cu2–O4) are imposed by the Jahn–Teller active electronic configuration (Table 2).

A pattern of edge- and corner-sharing of oxygen atoms between copper and molybdate coordination polyhedra, and edge-sharing directly between the copper coordination polyhedra, creates a 1-D copper molybdate ribbon motif that propagates parallel to the *b* crystal direction (Fig. 2a). Each Cu1 atom sitting on the periphery of the ribbon edge-shares two oxygen atoms (O2, O6) with Cu2 atoms positioned towards the interior of the ribbon, wherein two adjacent Cu2 atoms edge-share the same set of two O9 oxygen atoms. Thus, a kinked $\{Cu_4O_6\}$ tetramer is constructed, with consecutive Cu···Cu distances of 3.157, 3.052, and 3.157 Å (Fig. 2b). These tetramers are further stabilized by Mo1 molybdate units, which bridge both Cu2 atoms through oxygen atoms O4 and O2 in a corner-sharing mode. The sides of the ribbon are constructed by Mo1 molybdate dianions, which engage in corner-sharing of the doubly bridging atom O5 with one Cu1 atom, and corner-sharing of the triply bridging oxygen atom O2 with another Cu1 atom. The interior Cu2 atoms within the

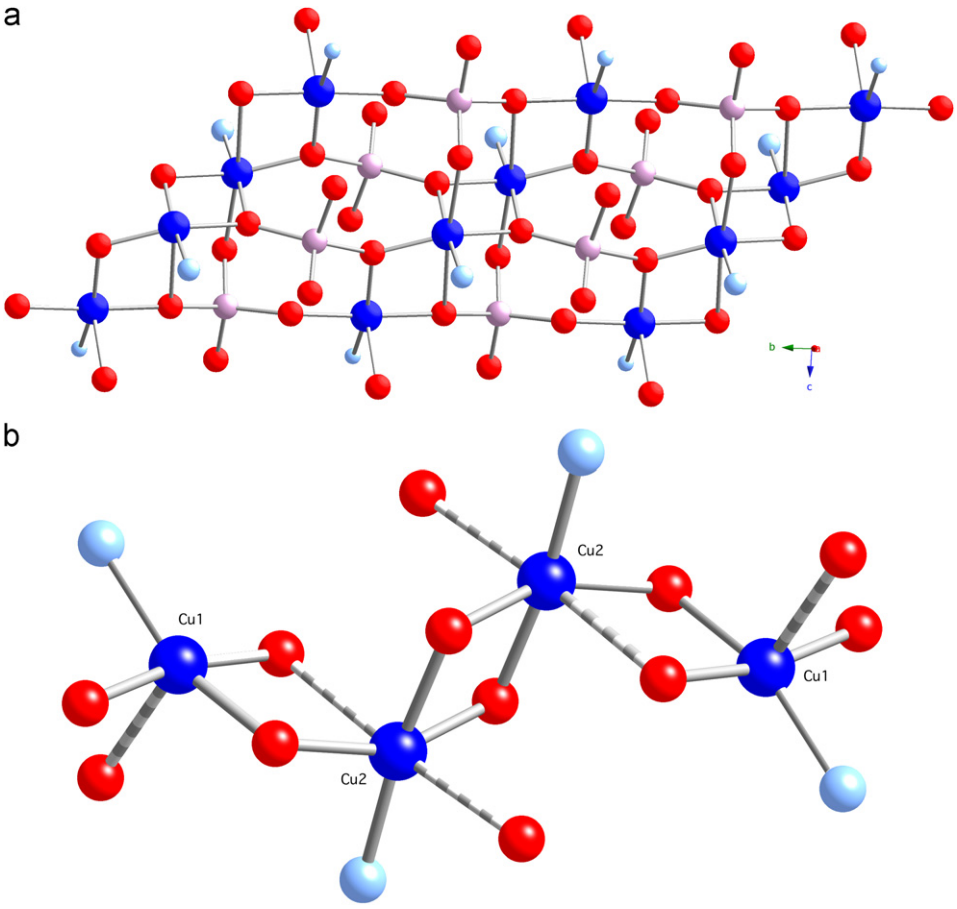

Fig. 2. (a) A copper molybdate ribbon in **1**, viewed down the *a* crystal axis. (b) A $\{Cu_4O_6\}$ tetrameric unit in **1**, with complete coordination spheres shown. The "long" bonds to axial coordination sites are depicted as dashed lines.

tetrameric kernels are connected to Cu2 atoms in two neighboring tetrameric units along the ribbon by Mo2 molybdate dianions (via O6 and O9). Nitrogen atoms from 3,4′-dpk ligands and ligated water molecules decorate the sides of the ribbon. The Cu1···Cu1 and Cu2···Cu2 distances between individual $\{Cu_4O_6\}$ tetramers are both 6.950(1) Å, which define the *b* lattice parameter.

Adjacent ribbons link into $[Cu_2(MoO_4)_2(3,4'\text{-dpk})(H_2O)]_n$ layers, parallel to the *bc* crystal planes, by means of tethering 3,4′-dpk ligands (Fig. 3). The 4′-termini of the 3,4′-dpk ligands bind solely to the Cu1 atoms on the edge of the ribbon motif. The ligands then weave above and below the plane of the layer, connecting to Cu2 atoms in the interior of neighboring ribbons via their 3-position nitrogen atoms. Fostering a Cu1···Cu2 interribbon through ligand distance of 8.357 Å, the 3,4′-dpk units adopt a twisted conformation with an inter-ring torsion angle of 39.1°. The 2-D covalent connectivity is supplemented by hydrogen bonding interactions between the aquo ligand hydrogen atoms (H10A) and the terminal oxo group at Mo1 (O3).

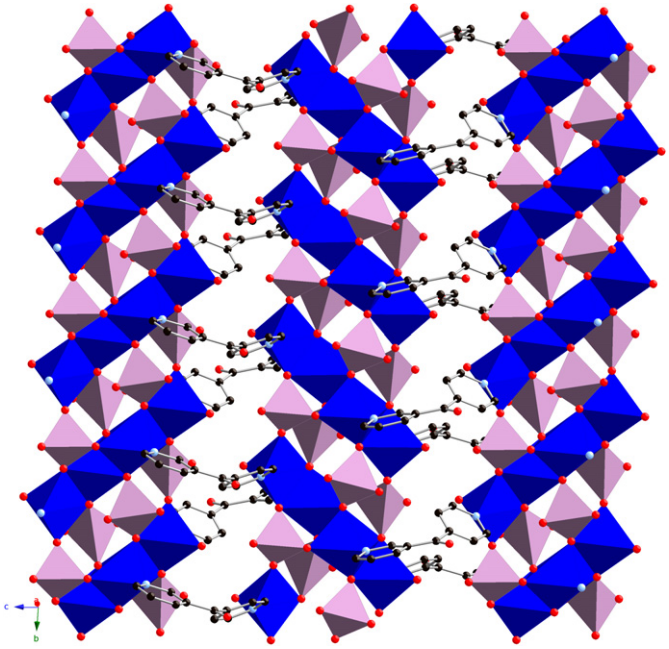

Fig. 3. A 2-D $[Cu_2(MoO_4)_2(3,4'\text{-dpk})(H_2O)]$ layer in **1**, viewed down the *a* crystal axis.

Discrete $[Cu_2(MoO_4)_2(3,4'\text{-dpk})(H_2O)]_n$ layers stack along the *a* crystal direction through hydrogen bonding pathways provided by the aquo ligands (via H10B) and the ketone functional groups of the 3,4′-dpk ligands (Fig. 4). Geometrical parameters for the hydrogen bonding patterns in **1** are given in Table 3. The nearest Cu1···Cu1 contact between $[Cu_2(MoO_4)_2(3,4'\text{-dpk})(H_2O)]_n$ layers is 10.391 Å, defining the *a* lattice parameter.

The 2-D structural morphology of **1** stands in contrast to the 3-D pillared networks seen in $\{[CuMoO_4(4,4'\text{-bpy})_{0.5}]\cdot 1.5H_2O\}$[3] and $[CuMoO_4(dpa)_{0.5}]$ [11], although all three of these materials contain $\{Cu_4O_6\}$ tetrameric subunits and individual $[MoO_4]^{2-}$ tetrahedra. In the latter two solids, the molybdate anions and copper ions construct 2-D $[CuMoO_4]_n$ layers. As a result, the oxygen atoms edge-shared between the copper atoms within the $\{Cu_4O_6\}$ tetramers occupy different coordination sites in **1** versus $\{[CuMoO_4(4,4'\text{-bpy})_{0.5}]\cdot 1.5H_2O\}$ and $[CuMoO_4(dpa)_{0.5}]$. In **1**, the edge-shared oxygen atoms between Cu1 and Cu2 both occupy equatorial sites on Cu1, but are split between axial and equatorial positions on Cu2. The oxygen atoms

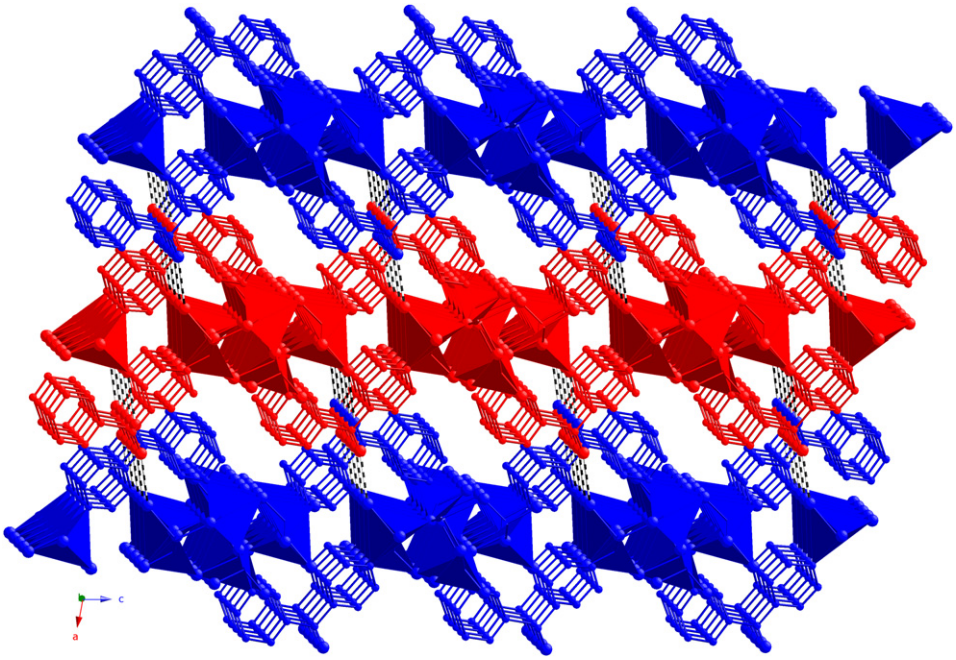

Fig. 4. Stacking of 2-D $[Cu_2(MoO_4)_2(3,4'\text{-dpk})(H_2O)]$ layers in **1**. Interlayer hydrogen bonding is indicated as dashed lines.

Table 3
Hydrogen bonding distance (Å) and angle (°) data for **1**

D–H···A	*d*(H···A)	<DHA	*d*(D···A)	Symmetry transformation for A
O10–H10A···O3	1.91(3)	169(11)	2.751(12)	$-x+1, y+1/2, -z+1/2$
O10–H10B···O1	2.16(8)	136(9)	2.829(11)	$x-1, y, z$

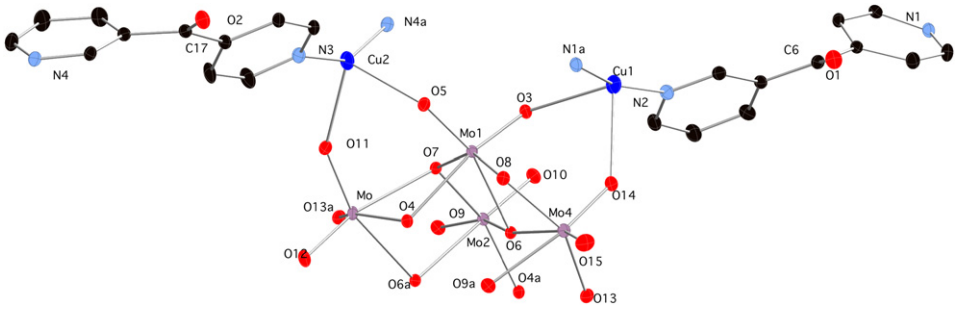

Fig. 5. Coordination environments in **2**, with thermal ellipsoids shown at 50% probability and partial atom numbering scheme. Hydrogen atoms have been omitted.

linking two Cu2 atoms in the center of the $\{Cu_4O_6\}$ tetramer occupy two equatorial sites within each Cu2 coordination octahedron (see Fig. 2b). In $\{[CuMoO_4(4,4'\text{-bpy})_{0.5}]\cdot 1.5H_2O\}$, all oxygen atoms shared between copper atoms in its $\{Cu_4O_6\}$ tetramers occupy an axial position on one Cu atom, and an equatorial site on another. This difference likely promotes differences in the magnetic behavior between **1** and $\{[CuMoO_4(4,4'\text{-bpy})_{0.5}]\cdot 1.5H_2O\}$ (see below).

4.3. *Structural description of* $[Cu_4(3,4'\text{-dpk})_4(\beta\text{-}Mo_8O_{26})]$ (**2**)

The asymmetric unit of compound **2**, which crystallizes in the centrosymmetric triclinic space group, consists of two crystallographically distinct monovalent copper atoms, one-half of an octamolybdate anion, and two 3,4′-dpk moieties (Fig. 5). Both of the copper atoms both display distorted "sawhorse" $[CuN_2O_2]$ coordination geometries, with bond angles about Cu1 ranging from 77.7° to 164.6°. The coordination sphere about Cu2 deviates more from a "sawhorse" to a tetrahedral arrangement, with bond angles ranging from 81.4° to 149.2°.

The flexible coordination environments are reflective of the lack of any crystal field stabilization for the d^{10} configuration monovalent copper ion. The nitrogen donor atoms at Cu1 belong to different termini of two different crystallographically identical 3,4′-dpk ligands (*dpk-A*, marked by atoms C1–C11/N1–N2/O1); terminal Mo = O molybdate oxygen atoms O3 and O14 are also bound to Cu1. A similar arrangement is observed for Cu2, with its nitrogen donor atoms provided by different termini of two *dpk-B* ligands (atoms C12–C22/N3–N4/O2). Terminal Mo = O molybdate oxygen atoms O5 and O11 round out the coordination sphere of Cu2. Operation of the crystallographic inversion center gives rise to a complete "dense" β-octamolybdate cluster, wherein all molybdenum atoms possess octahedral $[MoO_6]$ coordination environments that engage in mutual edge-sharing of oxygen atoms [9]. Pertinent bond lengths and angles for **2** are stated in Table 4.

Table 4
Selected bond distance (Å) and angle (°) data for **2**

Cu1–N2	1.9259(19)	N2–Cu1–N1$^{\#1}$	164.63(9)
Cu1–N1$^{\#1}$	1.9262(19)	N2–Cu1–O14	92.80(7)
Cu1–O14	2.4006(18)	N1$^{\#1}$–Cu1–O14	94.78(7)
Cu1–O3	2.4191(16)	N2–Cu1–O3	104.24(7)
Cu2–N4	1.925(2)	N1$^{\#1}$–Cu1–O3	90.44(7)
Cu2–N3$^{\#1}$	1.9283(19)	O14–Cu1–O3	77.75(6)
Cu2–O11	2.2137(18)	N4–Cu2–N3$^{\#1}$	149.20(9)
Cu2–O5	2.2894(17)	N4–Cu2–O11	111.35(8)
		Mo3–O11–Cu2	144.02(9)
		Mo4–O14–Cu1	136.28(9)

Symmetry equivalent atoms: (#1) $x-1, y, z$; (#2) $-x+1, -y+1, -z+1$.

Extension of the structure along the *a* crystal direction results in $[Cu_4(3,4'\text{-dpk})_4(\beta\text{-}Mo_8O_{26})]_n$ 1-D coordination polymer ribbon motifs (Fig. 6). Within these ribbons, individual $[\beta\text{-}Mo_8O_{26}]^{4-}$ polyoxoanions are connected through two $[Cu1(dpk\text{-}A)]_n$ 1-D chains and two $[Cu2(dpk\text{-}B)]_n$ 1-D chains that decorate their respective peripheries. Both Cu1···Cu1 and Cu2···Cu2 distances through the 3,4′-dpk ligands measure 10.900 Å, marking the *a* lattice parameter. Despite the identical metal–metal contact distances, the inter-ring torsion angles within the *dpk-A* and *dpk-B* ligands vary, subtending 57.7° and 49.2°, respectively. The Cu1···Cu1 and Cu2···Cu2 distances through a $[\beta\text{-}Mo_8O_{26}]^{4-}$ unit are 11.428 and 11.056 Å, respectively. Covalent connectivity within the 1-D ribbons is supplemented by π–π stacking interactions (centroid-to-centroid distance = 3.95 Å) between pyridyl rings in adjoining $[Cu(3,4'\text{-dpk})]_n$ chains.

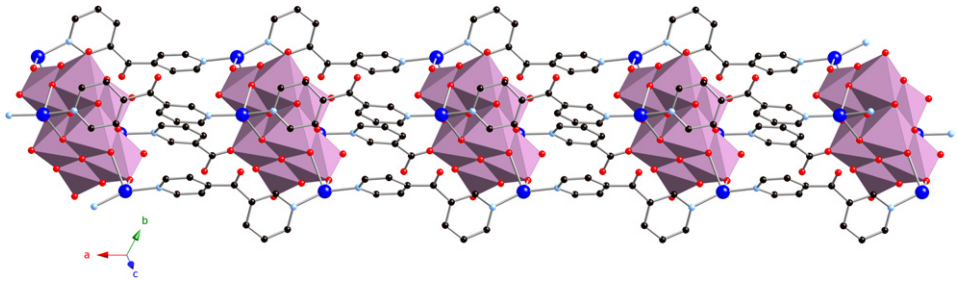

Fig. 6. A single $[Cu_4(3,4'\text{-dpk})_4(\beta\text{-}Mo_8O_{26})]_n$ 1-D coordination polymer ribbon. The polyoxomolybdate clusters are shown in a polyhedral representation.

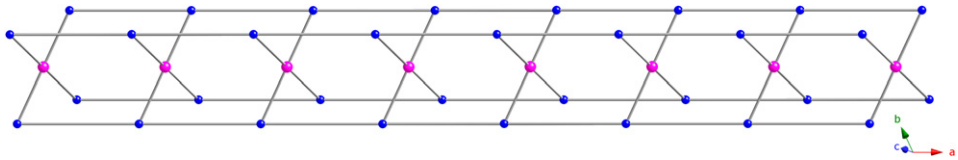

Fig. 7. A framework representation of the unprecedented (3,4)-connected $(6^28)_4(6^6)$ topology "X-rail" 1-D structural motif in **2**. The centroids of the $(\beta\text{-}Mo_8O_{26})^{4-}$ anions are shown as 4-connected nodes.

Each copper atom acts as a 3-connected node, joining to two other copper atoms through exobidentate 3,4′-dpk ligands and connecting directly to one $[\beta\text{-}Mo_8O_{26}]^{4-}$ polyoxoanion. As each polyoxomolybdate cluster connects four $[Cu(3,4'\text{-dpk})]_n^{n+}$ 1-D chains, a single cluster can be considered to be a 4-connected node. Thus, an unprecedented (3,4)-connected binodal $(6^28)_4(6^6)$ topology 1-D "X-rail" motif can be invoked (Fig. 7). Neighboring "X-rails" aggregate into the pseudo 3-D crystal structure of **2** primarily through weak C–H···O interactions (C5···O14, 3.160(4) Å; C20···O9, 3.112(4) Å). The closest inter-chain Cu···Cu contact distance is 5.073 Å.

4.4. Magnetic behavior of *1*

The variable temperature magnetic susceptibility behavior of **1** was investigated in order to probe spin communication within and between its $\{Cu_4O_6\}$ tetrameric kernels. At 298 K, the χ_mT product was 0.175 cm^3 K/mol Cu, beneath that expected for an uncoupled $S = 1/2$ ion with $g = 2.0$, potentially indicative of antiferromagnetic coupling. The χ_mT product increased on cooling, reaching a maximum value of 0.28 cm^3 K/mol Cu at 95 K, thereby revealing likely ferromagnetic interactions within the tetramers. Upon further cooling, the χ_mT value decreases rapidly, approaching negligible values at 2 K, thus marking the presence of net antiferromagnetism.

A Curie–Weiss plot of χ_m^{-1} vs. T (Fig. S1) was only remotely linear in the high temperature regime ($T > 200$ K). Linear regression of this data reveals $C = 0.100$ cm^3/mol K with the Θ of 124 K indicative of the presence of ferromagnetic coupling within the tetrameric units at elevated temperatures. The Curie constant is lower than expected, indicating antiferromagnetic behavior within or between the tetrameric units. For a more accurate treatment, the susceptibility data was fit to an equation (Eq. (1)) developed by Rubenacker and colleagues [19] from the Hamiltonian for a Heisenberg $S = 1/2$ linear tetramer (Eq. (2)), including a mean field inter-tetramer interaction term zJ' and a correction for temperature independent magnetic susceptibility (χ_{TI}). Exchange parameters between Cu1 and Cu2 atoms on the edges of the tetramer, and between Cu2 atoms at the center of the tetramer, are defined as J_1 and J_2, respectively. Best fit parameters were as follows: $g = 2.03(3)$, $J_1 = 25.8(7)$ cm^{-1}, $J_2 = -46(1)$ cm^{-1}, $zJ' = -0.21(3)$ cm^{-1}, $\chi_{TI} = -0.00082(1)$ cm^3/mol, with $R = 4.3 \times 10^{-3} = \{\Sigma[(\chi_mT)_{obs} - (\chi_mT)_{calc}]^2/[(\chi_mT)_{obs}]^2\}^{1/2}$ (Fig. 8),

$$\chi'_m = \left(\left\{\frac{Ng^2\beta^2}{4kT}\right\} \times \left[\frac{10e^{(-E_1/kT)} + 2e^{(-E_2/kT)} + 2e^{(-E_3/kT)} + 2e^{(-E_4/kT)}}{5e^{(-E_1/kT)} + 3e^{(-E_2/kT)} + e^{(-E_3/kT)} + e^{(-E_4/kT)} + e^{(-E_5/kT)} + e^{(-E_6/kT)}}\right] + \chi_{TI}\right), \quad (1)$$

where

$$E_1 = -J_1 - (J_2/2); \quad E_2 = J_1 - (J_2/2);$$

$$E_3 = (J_2/2) + \sqrt{J_1^2 + J_2^2};$$

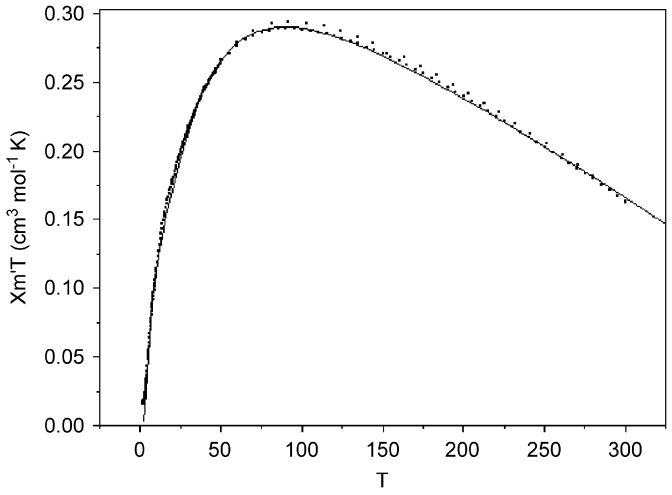

Fig. 8. Plot of $\chi_m T$ vs. T for **1**. The solid line indicates the best fit to Eq. (1) in the text.

$$E_4 = (J_2/2) - \sqrt{J_1^2 + J_2^2};$$

$$E_5 = J_1 + (J_2/2) + \sqrt{4J_1^2 - 2J_1J_2 + J_2^2};$$

$$E_6 = J_1 + (J_2/2) - \sqrt{4J_1^2 - 2J_1J_2 + J_2^2}$$

with

$$\chi_m T = \left(\frac{\chi'_m}{1 - (2zJ'\chi'_m/Ng^2\beta^2)}\right)T$$

$$H = -2J_1(\vec{S}_1\vec{S}_2 + \vec{S}_3\vec{S}_4) - 2J_2(\vec{S}_2\vec{S}_3). \quad (2)$$

Thus, the interaction between the external and internal Cu atoms within a single tetramer in **1** is ferromagnetic, while antiferromagnetic coupling is extant between internal Cu atoms. The negative zJ' value indicates the likely presence of antiferromagnetic interactions between tetrameric $\{Cu_4O_6\}$ units via the molybdate anions, along the 1-D metal oxide ribbons in **1**. It is very likely that magnetic superexchange through the longer 3,4′-dpk spacers is negligible in comparison. An antiferromagnetic $S = 0$ ground state for the $\{Cu_4O_6\}$ units is corroborated by an examination of the χ_m vs. T plot, which reveals a maximum in the susceptibility curve at $T \sim 10$ K.

The magnetic interaction pattern in **1** is different from that seen in $\{[Cu(4,4'\text{-bpy})_{0.5}MoO_4]\cdot 1.5H_2O\}$, which also possesses $\{Cu_4O_6\}$ tetrameric subunits. In this latter material, only antiferromagnetic interactions within the tetramers are evident. Ruiz-Perez and co-workers have posited that magnetic superexchange in copper coordination polymers is very dependent on the geometric orientation of the magnetic d_{x2-y2} orbitals on adjacent Cu ions, with *equatorial–equatorial* bridging patterns maximizing this interaction [20]. Therefore the differences in the coordination sites occupied by edge-shared oxygen atoms within the $\{Cu_4O_6\}$ tetramers in **1** and $\{[Cu(4,4'\text{-bpy})_{0.5}MoO_4]\cdot 1.5H_2O\}$ are the probable origin for the divergent magnetic behavior between these materials.

5. Conclusion

Hydrothermal synthesis has permitted the self-assembly of two copper molybdate phases with novel morphologies, based on the kinked tethering organodiimine 3,4′-dpk. Compounds **1** and **2** represent the first coordination polymers to include this ligand, and could be selectively prepared through careful control of the initial pH of the reaction mixture. A unique "infinite" 1-D $\{CuMoO_4\}$ ribbon is constructed from $\{Cu_4O_6\}$ tetrameric units in **1**, which display cooperative antiferromagnetic and ferromagnetic behavior within and between tetramers. In turn these ribbons are conjoined into a 2-D coordination polymer layer through the tethering 3,4′-dpk ligands, whose central ketone moieties promote critical inter-layer supramolecular interactions. The reduced phase **2** manifests standard β-octamolybdate anions, linked into a unprecedented (3,4)-connected "X-rail" 1-D coordination polymer through $[Cu(3,4'\text{-dpk})]_n^{n+}$ chains. Efforts to prepare other mixed metal oxide and dicarboxylate coordination polymers that incorporate 3,4′-dpk are underway in our laboratory, seeking to take further advantage of this ligand's unique covalent bonding and supramolecular interaction patterns.

6. Supplementary material

Crystallographic data for **1** and **2** have been deposited with the Cambridge Crystallographic Data Centre with the deposition numbers 662259 and 662260, respectively. Copies of the data can be obtained free of charge via the Internet at http://www.ccdc.cam.ac.uk/conts/retrieving.html or by post at CCDC, 12 Union Road, Cambridge CB2 1EZ, UK (Fax: 44 1223336033, Email: deposit@ccdc.cam.ac.uk). Additional magnetochemical plots for **1** are available via the online version of this article at doi:10.1016/j.jssc.2008.01.036.

Acknowledgments

The authors gratefully acknowledge Michigan State University for financial support of this work. We thank Dr. Rui Huang (MSU) for elemental analysis and Mr. Paul Szymanski for acquisition of the infrared spectra. We especially thank one of the reviewers for keen insight into the magnetic studies, SDG.

Appendix A. Supplementary materials

Supplementary data associated with this article can be found in the online version at doi:10.1016/j.jssc.2008.01.036.

References

[1] (a) N.N. Greenwood, A. Earnshaw, Chemistry of the Elements, Pergamon Press, New York, 1984;
(b) W. Büchner, R. Schiebs, G. Winter, K.H. Büchel, Industrial Inorganic Chemistry, VCH, New York, 1989;
(c) B. Cockayne, D.W. Jones, in: D.W. Jones (Ed.), Modern Oxide Materials, Academic Press, New York, 1972;
(d) W.H. McCarroll, in: R.B. King (Ed.), Encyclopedia of Inorganic Chemistry, vol. 6, Wiley, New York, 1994, pp. 2903–2946;
(e) A.K. Cheetham, Science 264 (1994) 794;
(f) P.J. Hagrman, D. Hagrman, J. Zubieta, Angew Chem., Int. Ed 38 (1999) 2638 and references therein.

[2] (a) X.Y. Hu, J.C. Yu, J.L. Gong, Q. Li, G. Li, Guisheng. Adv. Mater. 19 (2007) 2324;
(b) W.G. Menezes, D.M. Reis, M.M. Oliveira, J.F. Soares, A.J.G. Zarbin, Chem. Phys. Lett. 445 (2007) 293;
(c) S.H. Lee, T.W. Kim, D.H. Park, J.-H. Choy, S.-J. Hwang, N. Jiang, S.-E. Park, Y.-H. Lee, Chem. Mater. 19 (2007) 5010;
(d) S. Chen, H. Ma, S. Xiang, X. Yi, Smart Mater. Struct. 16 (2007) 696.

[3] R. Rarig, R. Lam, P. Zavalij, J. Ngala, J. Katana, R. LaDuca, J. Greedan, J. Zubieta, Inorg. Chem. 41 (2002) 2124.

[4] D. Hagrman, C. Sangregorio, C.J. O'Connor, J. Zubieta, J. Chem. Soc., Dalton Trans. (1998) 3707.

[5] R.S. Rarig, J.A. Zubieta, Polyhedron 22 (2003) 177.

[6] D. Hagrman, P. Hagrman, J. Zubieta, Inorg. Chim. Acta 300–302 (2000) 212.

[7] C.E. Ochalek, R.L. LaDuca, Acta Cryst. E 63 (2007) m621.

[8] D. Hagrman, C. Zubieta, R.C. Haushalter, J. Zubieta, Angew Chem., Int. Ed. 36 (1997) 873.

[9] D.G. Allis, R.S. Rarig, E. Burkholder, J. Zubieta, J. Mol. Struct. 688 (2004) 11.

[10] R.S. Rarig, L. Bewley, E. Burkholder, J. Zubieta, Ind. J. Chem. 42A (2003) 2235.

[11] D. Hagrman, C.J. Warren, R.C. Haushalter, C. Seip, C.J. O'Connor, R.S. Rarig, K.M. Johnson, R.L. LaDuca, J. Zubieta, Chem. Mater. 10 (1998) 3294.

[12] X.-D. Chen, T.C.W. Mak, J. Mol. Struct. 743 (2005) 1.

[13] O. Khan, Molecular Magnetism, VCH Publishers, New York, 1993.

[14] SAINT, Software for Data Extraction and Reduction, Version 6.02, Bruker AXS, Inc., Madison, WI, 2002.

[15] SADABS, Software for Empirical Absorption Correction, Version 2.03, Bruker AXS, Inc., Madison, WI, 2002.

[16] G.M. Sheldrick, SHELXTL, Program for Crystal Structure Refinement, University of Gottingen, Gottingen, Germany, 1997.

[17] A.L. Spek, PLATON, A Multipurpose Crystallographic Tool, Utrecht University: Utrecht, The Netherlands, 1998.

[18] A.W. Addison, T.N. Rao, J. Chem. Soc., Dalton Trans. (1984) 1349.

[19] (a) G.V. Rubenacker, J.E. Drumheller, K. Emerson, R.D. Willett, J. Magn. Magn. Mater. 54–57 (1986) 1483;
(b) J.A. Ayllon, I.C. Santos, R.T. Henriques, M. Almeida, L. Alcacer, M.T. Duarte, Inorg. Chem. 35 (1996) 168.

[20] J. Pasan, F.S. Delgado, Y. Rodriguez-Martin, M. Hernandez-Molina, C. Ruiz-Perez, J. Sanchiz, F. Lloret, M. Julve, Polyhedron 22 (2003) 2143.